ELSEVIER

Journal of Alloys and Compounds 452 (2008) 325–335

Journal of ALLOYS AND COMPOUNDS

www.elsevier.com/locate/jallcom

The strain energy and shape evolution of hydrides precipitated at free surfaces of metals

Y. Greenbaum [a], D. Barlam [b], M.H. Mintz [a,d], R.Z. Shneck [c,*]

[a] *Department of Nuclear Engineering, Ben-Gurion University of the Negev, Beer Sheva, P.O. Box 653, Israel*
[b] *Department of Mechanical Engineering, Ben-Gurion University of the Negev, Beer Sheva, P.O. Box 653, Israel*
[c] *Department of Materials Engineering, Ben-Gurion University of the Negev, Beer Sheva, P.O. Box 653, Israel*
[d] *Nuclear Research Center-Negev, P.O. Box 9001, Beer Sheva, Israel*

Received 20 September 2006; received in revised form 9 November 2006; accepted 9 November 2006
Available online 22 December 2006

Abstract

The volume changes, which are associated with hydride formation involve large strain energy. In the present work, Finite Element calculations of the strain energy of hydrides formed at the free surface of a metal matrix is done as function of several variables: the shape of the hydride precipitate, the elastic anisotropy of the crystals with cubic symmetry, the elastic heterogeneity, elastic–plastic transition and the effect of an oxide layer on the surface. The effect of these variables on the kinematics of the elastic strains and on the distribution of the energy between the matrix and hydrides are used to interpret the results and to deduce the preferred shapes, those having the lowest energy.

The elastic energy of half-spherical hydrides at the surface is found to be minimal in most of the elastic and elastic–plastic systems considered (due to different reasons). A plate-shaped hydride with broad face parallel to the free surface may become preferred in an elastic matrix if the hydride is significantly softer than the matrix, or its broad face is parallel to a soft crystallographic plane. The existence of a thick oxide layer over the free surface increases the total energy of the system and moderates the dependence of the energy on the shape. As the hydride grows, the preference of the spherical shape is enhanced. For the case of a plastic matrix covered with an oxide layer, the preferred growth shape changes from a sphere to an elongated precipitate perpendicular to the free surface.

Keywords: Metal hydrides; Precipitation; Thermodynamic modeling; Anisotropy; Strain

1. Introduction

The initial stages of gas–solid reactions, e.g., oxidation, hydrating, etc., frequently involve the nucleation and growth of the reaction product (as precipitates) at the surface or at the near-surface region. In many cases, like hydride precipitates to which we refer in this work, the density of the product is lower than that of the parent material therefore a volume expansion accompanies the growth of the precipitates setting up stresses in the hydride and around it. These stresses are associated with strain energy, which affects the growth of the product particles and gives rise to interaction with other stress-sources like dislocations [1,2], oxide layers and other hydrides. Thus, the strain energy may have a significant effect on the hydrogen–metal reaction.

An example for this situation was observed by Bloch et al. [3] during hydrogenation of uranium. Multiple hemispherical hydrides nucleate, sometime preferably along slip lines. Most of them cease to grow but a few grow into large precipitates [4–6]. Bloch et al. [3] suggested that the increase in elastic energy accumulated during the growth process causes the interception of the growth. The growth proceeds only where the oxide layer that covers the metal surface breaks.

Elastic effects associated with second phase particles have been intensively investigated in *bulk materials*. They can affect the shape, size and orientation of particles [7]. In extreme cases, e.g., martensitic transformations, the elastic energy can retard the transformation or cause internal deformation in the new phase particles [7,8]. Elastic interaction among second-phase particles can induce ordering of the new phase in bulk materials [e.g., 7] as well as on free surfaces [e.g., 9]. Since the role of the elastic energy in the evolution of the microstructure of solid materials was recognized, a special

* Corresponding author. Tel.: +972 86472493; fax: +972 86472946.
E-mail address: roin@bgu.ac.il (R.Z. Shneck).

0925-8388/$ – see front matter © 2006 Elsevier B.V. All rights reserved.
doi:10.1016/j.jallcom.2006.11.045

branch was developed in solid mechanics to study these phenomena.

The first attempt to calculate the elastic energy of a precipitate by continuum approach was published by Nabarro [10]. He was able to solve the elastic field under the assumption that the precipitate behaves like a "fluid in a cavity", that is hydrostatically stressed. This resembles an incoherent precipitate, which has broken bonds with the matrix.

The problem was extended by several authors to coherent precipitates of specific shapes, for which continuity of the displacements and tractions across the precipitate–matrix interface was assumed [see refs. in 11] until Eshelby [12] suggested a solution to the elastic fields associated with a coherent "inclusion" with an arbitrary shape and misfit (transformation) strains. The restrictions of his solution are to infinite, isotropic and homogeneous (equal elastic constants of the matrix and the particle) systems. The solution was obtained by integration of Green functions. Asaro and Barnett [13], applied Green functions for anisotropic materials. An alternative approach to solve the homogenous, anisotropic inclusion problem in infinite matrix was suggested by Mura [14] and Khachaturyan [7]. They used the Fourier transform to solve the equilibrium equations.

The restriction to infinite matrix was removed by several authors, who solved problems of precipitates near a free surface. They are interesting in the context of reactions of solids with gases and of nanostructures such as "quantum wires" and "quantum dots". Four approaches have been advised to fulfill the free surface boundary conditions in homogenous isotropic materials by applying image forces:

(a) Integration of the Green function for half-space [15–17].
(b) Expressing the solution as Fourier transform [18–20].
(c) Summation of elementary solutions obtained by Fourier method. It was applied for cylindrical and rectangular "wires" [21].
(d) Application of the Hankel transform and superposition [22].

Recently a Green function for anisotropic half-space was devised [23].

It is believed that the shape of precipitates is determined by the tendency of the system to follow a path of lowest energy. This question was thoroughly discussed for precipitates in infinite matrix since the pioneering work of Nabarro. In isotropic homogenous systems the energy per unit volume does not vary with the shape if the misfitting strains are *pure dilatational* [10–12]. Laszlo [24] showed that in heterogeneous, isotropic system a plate-shaped particle is associated with the minimum elastic energy if its shear modulus is smaller than that of the matrix. Otherwise a spherical particle is the favored shape. Lee et al. [25] and Shneck et al. [26] generalized this criterion for cubic anisotropy. They found again that either a plate-shape (parallel to the $\{1\,0\,0\}$ or the $\{1\,1\,1\}$ plane) or a sphere-shape are associated with minimum elastic energy. Later Suh and Park [27] found that needles might also have minimum energy at certain conditions. They proposed the use of stability diagrams to map the range of parameters where each precipitate shape is stable.

For more general transformation strains there is a controversy. While Khachturyan [7] claimed that a plate-shape is always the shape of minimum energy in a homogenous system, Roitburd [28] suggested stability maps containing different shapes for different tetragonal misfit. Dahmen and Westmacott [29] showed that observed precipitates grow parallel to invariant lines or invariant planes when the transformation strains contain such features.

Systematic investigation of the variation of the elastic energy with the shape of precipitates *near a free surface* is lacking. Homogeneous systems can be solved analytically [15–22] but analytic solutions for inhomogeneous and anisotropic problems near a free surface become intractable. Numerical methods, in particular the Finite Element Method (FEM) enable the solution of such mechanical problems with complicated material behavior and boundary conditions. The FEM is applied here to find the strain energy of precipitates with pure dilatational transformation strains, growing near the free surface of an infinite half-space. Some experimentally important situations are modeled, including analysis of the effect of anisotropy, of heterogeneity of the elastic constants and of an oxide layer covering the surface. The solutions are found for a representative series of half-ellipsoidal particles, from which the preferred shapes associated with the minimum elastic energy are determined. The displacement and stress fields given rise by the precipitate are studied to interpret the results.

The material behavior is first assumed to be linear elastic. Many phase transformations are associated with large transformation strains. In particular, hydride formation may be associated with misfit strains of the order of 10%. Therefore, the calculation where repeated for hyperelastic material with kinematics taking account of the large strains. Real metals undergo plastic yielding under large stresses. This discontinuous change in the constitutive behavior of the material that is studied in the last part of the work. Another feature of practical importance is the occurrence of oxide layer on the metal surface. The effect of the stiff oxide layer on the preferred shape of the hydride is calculated for elastic and elastic–plastic materials.

2. Method and modeling

The strain energy of coherently bonded hydrides at a free surface of a solid was calculated as function of their shape. The calculations were performed by the FEM applying the MSC. NASTRAN code. A spherical segment was modeled taking in consideration the axial symmetry of the problem (10° for isotropic material containing 1575 elements and 90° for cubic materials containing 14175 elements, see Fig. 4a). The hydrides are assumed to have the shape of half-ellipsoids with radii $a = b$ parallel to the x- and y-directions on the free surface and c-axis parallel to the z-direction normal to the free surface. For anisotropic systems, the crystallographic axes of the matrix and precipitate were assumed parallel to each other. The shape varied parametrically from a flat ellipsoid to an elongate one with principle axes along x,y,z-directions. The dimensions of the hydride varied between 5.5 and 90 times smaller than the matrix radii in the model. Pure dilatational misfit (transformation) strains are assumed ($\varepsilon_{ij}^{\mathrm{T}} = \varepsilon^0 \delta_{ij}$), represented by thermal strains in the hydride.

The elastic energy (W) was found in the framework of linear elasticity by calculating the sum [12]:

$$W = \frac{1}{2}\int_{V_{\mathrm{m}}} \sigma_{ij}\varepsilon_{ij}^{\mathrm{c}}\ \mathrm{d}V + \frac{1}{2}\int_{V_{\mathrm{p}}} \sigma_{ij}(\varepsilon_{ij}^{\mathrm{c}} - \varepsilon_{ij}^{\mathrm{T}})\ \mathrm{d}V \tag{1}$$

where V_{m} and V_{p} are the volumes of the matrix and the hydride respectively, $\varepsilon_{ij}^{\mathrm{c}}$ are the constraint strains measured relative to the initial state of the hydride and σ_{ij} are the elastic stresses.

Table 1
The elastic modulii of the materials used for the calculations

	M_1	M_2	Pd [32]	M_3	MO
C_{11} (GPa)	66.9	57.2	223.28	83	141.3
C_{12} (GPa)	23.4	28	173.12	21	49.4
C_{44} (GPa)	21.8	29.2	71.25	15.5	45.9
A	1	2	2.84	0.5	1

Metal	σ_{uts} (MPa)	σ_{yp} (MPa)	ε_l (%)	$\varepsilon_{V\,hydride}$ (%)	$\varepsilon_{L\,hydride}$ (%)	$B_{hydride}$ (GPa)
Gd [30]	118	15	37	20 [34]	6	80 [33]

M_1 resembles polycrystalline Gd [30]. MO resembles Gd_2O_3 [31]. $A = 2C_{44}/(C_{11}-C_{12})$ is the parameter of anisotropy. ε_V and ε_L are the volumetric and linear misfit strains respectively.

The reported elastic energies are normalized to a unit transformation strain ε^0 and a unit volume of the precipitate. They were compared to results for precipitates in an infinite matrix obtained semi-analytically by the Fourier transformation method [14].

The elastic constants used for each specific model system are listed in Table 1. They are based on the properties of polycrystalline gadolinium (M_1). Two sets of constants of hypothetic cubic materials M_2 and M_3 where chosen with different anisotropy. Their elastic constants were determined such that the elastic energies associated with spherical precipitates formed in infinite homogenous materials M_1, M_2 and M_3 are all equal (Fig. 3a). The column Pd contains the elastic constants of palladium that were used in some calculations.

Non-linear material behavior was described by two models:

(a) Neohookean hyperplasic model with kinematics of large displacements and large strains. The model constants D and A_{10} were calculated from the elastic constants B (bulk modulus) and μ (shear modulus) by $2D_1 = B$; $2A_{10} = \mu$ [35].
(b) Elasto-plastic materials obeying the Von-Mises yield criterion with linear hardening rate of $(\sigma_{uts} - \sigma_{yp})/\varepsilon_l$. When the matrix yielded, the plastic work was calculated by:

$$W_m = \int_{V_m} \sigma_{ij}\varepsilon_{ij}^{pl}\, dV. \quad (2)$$

3. Results

3.1. Behavior in an infinite homogenous material

The elastic energy accumulated in the hydride–matrix system is maximal if the hydride is formed in an infinitely rigid matrix. The energy of such an unrelaxed hydride is:

$$E_{max} = \frac{3}{2}B(\varepsilon^0)^2 V_p \quad (3)$$

where B is the bulk elastic modulus of the hydride and V_p the volume of the hydride [12]. In actual matrices, the precipitates are allowed to relax until equilibrium is attained. At equilibrium, the stresses that remain in the precipitate are balanced by the stresses set up in the matrix and at the same time, the total elastic energy in the material decreases to the minimum. Eshelby [12] has shown that the elastic energy associated with a homogeneous, isotropic, coherent precipitate in an infinite matrix is independent of the shape of the precipitate. The partition of the energy between the matrix and the precipitate depends, however, on the precipitate shape. This partition will be discussed for the shapes of plate (Fig. 1a), sphere (Fig. 1b) and a needle-shaped hydride (Fig. 1c), in the case of pure dilation transformation strain.

Figs. 1b–d contain three maps of the displacements associated with three ellipsoidal hydrides of different shapes embedded in an *infinite* matrix. The strains are uniform in each hydride as first found by Eshelby [12]. Fig. 1a and b show two *plate*-shaped hydrides with pure dilatational transformation strains. The outstanding feature of Fig. 1b is the large difference between the wide dimension and the narrow one. The plate is constrained to the matrix lattice in its broad face (along x-axis in the illustration) and is relaxed along the thickness direction (z-axis). In Fig. 1a, a hypothetical hydride is shown that is less constrained in the broad face. Considerable displacements accumulate along the broad face of the plate, setting up large and long-range strains in the matrix, due to the continuity of the displacements between the matrix and the hydride. Hence, in the real dilating hydride (Fig. 1b), minimization of the strain energy of the coherent system is obtained by keeping the expansion in the broad face smaller, as the plate grows wider. Thus, high two-dimensional compressive stresses prevail in the broad plane of the plate. On the other hand, Fig. 1b shows large expansion of the hydride in its narrow dimension. The magnitude of the strain approximates the sum of the transformation strain in the z-direction, ε_{zz}^T, and the Poisson's expansion $-\upsilon(\varepsilon_{xx} + \varepsilon_{yy})$ that ensues from the high compression in the two lateral directions. The figure shows that since this large expansion is allowed only in the narrow dimension of the plate, the strains, which are enforced into the matrix are of short range. In summary, when the hydride is a very thin plate, the large part of the elastic energy accumulates in a two dimensional hydrostatic stress field within the plate. Only a small portion of the strains and elastic energy are transferred to the matrix.

The anisotropy of the stress fields decreases when the aspect ratio of the precipitate, $\beta = a/c$, approaches unity. The precipitate will be able to expand more in its wide dimensions, but will expand less in the narrow dimension. Hence, the expansion of a *spherical* precipitate (Fig. 1c) is uniform in all directions. A sphere is a compact, rigid shape and it enforces high strains on the matrix, therefore a large part of the elastic energy is transferred to the matrix.

When the aspect ratio of the precipitate continues to increase, the c-axis becomes larger then the a- and b-axes, describing a *needle*-shaped ellipsoid (Fig. 1d). As the c-axis increases the coherency constraints along the long z-axis increases, therefore the stress σ_{zz} in the hydride increases (Fig. 2a). Concurrently with the relative shortening of the a- and b-axes, the stresses

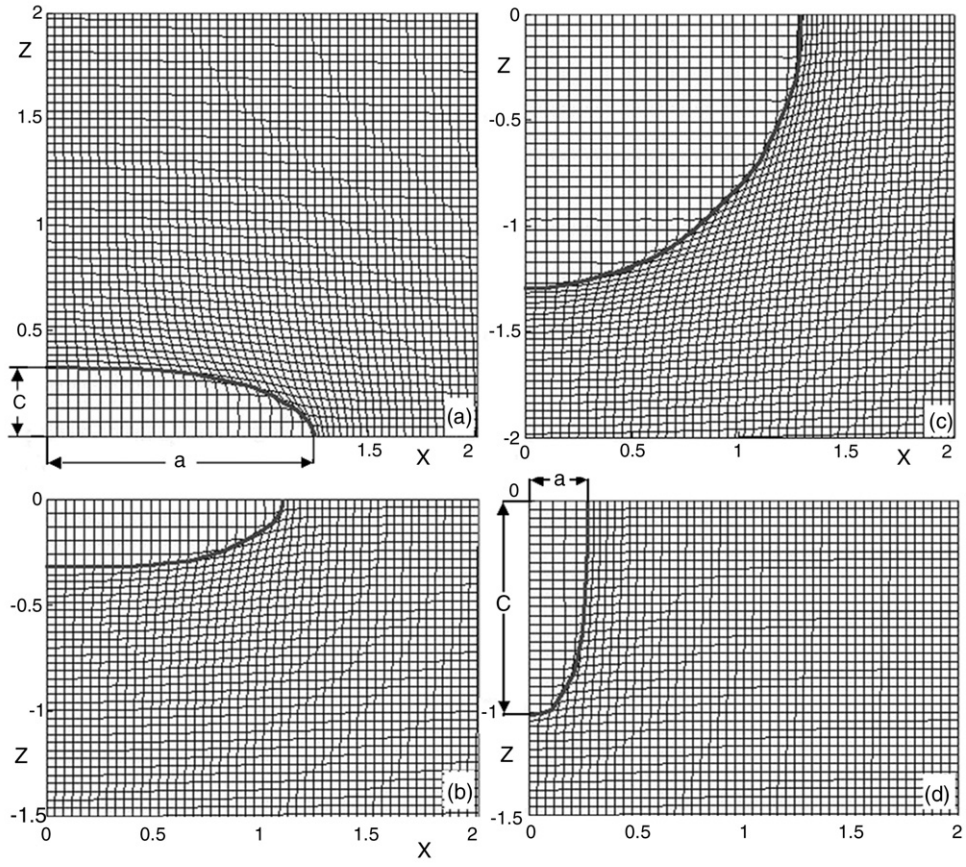

Fig. 1. Maps of displacements associated with three shapes of hydrides formed in an infinite isotropic matrix. The deformation is visualized by the displacement of a cubic grid of lines, which was inscribed in the material prior to the formation of the hydrides. Only the x–z plane of the grid is drawn. The transformation strains are $\varepsilon_{ij}^{T} = 0.5\delta_{ij}$, exaggerated in purpose to induce noticeable strains. The boundaries between the hydrides and the matrices are designated by a heavy line. The shapes of the hydrides are ellipsoidal with radii $a = b \neq c$ and principle axes parallel to the grid lines and the coordinates x,y,z. (a and b) A disk shaped hydride with $c/a = 0.2$ and broad face parallel to the x–y plane. (c) A spherical hydride ($c/a = 1$). (d) A needle-shaped hydride with $c/a = 5$ and long axis parallel to the z-axis. (a) A hypothetical hydride that expands laterally more than the real equilibrium state, shown in (b). Homogenous elastic constants of M_1 are assumed. Calculated by the semi-analytic Fourier method.

relax along x- and y-directions (Fig. 2b). Hence, the long axes are always more constrained and highly stressed, whereas the short axes are less constrained and therefore less stressed. Comparing the strains along the short axes of a plate-shape hydride to those in a needle-shaped one, shows that the plate is more relaxed (Figs. 1b and d). Figs. 2a and b indeed show that σ_{zz} in the plate is lower than σ_{xx} in the needle-shaped hydride having a reciprocal aspect ratio. The sum of the elastic energies in the hydride and in the matrix in infinite isotropic and homogenous systems is shown by curve 1 in Fig. 3a to be independent of the precipitate shape.

In elastically heterogeneous systems, the total energy depends on the shape of the hydride. Given that the hydride is softer than the matrix, the minimal energy resides with the hydride shape for which the major part of the elastic energy is accumulated in the hydride. This is the situation when the hydride is plate-shaped (curve 5 in Fig. 3a). On the other hand, if the matrix is softer than the hydride, the preferred shape will be spherical since in this case the majority of the energy resides in the matrix (curve 4).

The total energy depends on the shape also when the materials are anisotropic. In materials with cubic symmetry and $A > 1$ the planes $\{1\,0\,0\}$ are elastically soft. Thus, the energy is smallest in a system containing a plate-shaped precipitate with its broad face parallel to one of the $\{1\,0\,0\}$ planes (curve 2 in Fig. 3a). When $A < 1$ the planes $\{1\,0\,0\}$ are hard and the energy of such plate-shaped hydrides is high (curve 3 in Fig. 3a). In summery, the elastic energy in the case of infinite matrix creates preference only to the shapes of a plate or a sphere (for further details see Ref. [26]).

3.2. Mechanical behavior in a half-space

3.2.1. State of stress in a homogenous system

Figs. 4b–d contains three maps of the displacements associated with three of the modeled half-ellipsoidal hydrides at the free surface of a matrix. Fig. 5 compares the stress profiles in an infinite matrix to those in a half infinite matrix. The creation of the free surface enforces the σ_{zz} components of the stress to vanish at the surface. This allows the relaxation of the hydride near a free surface in the direction normal to the surface. In a needle-shaped hydride, the compressive σ_{zz} component gradually increases along the long z-axis due to the increasing constraints far from the free surface, converging to the stress

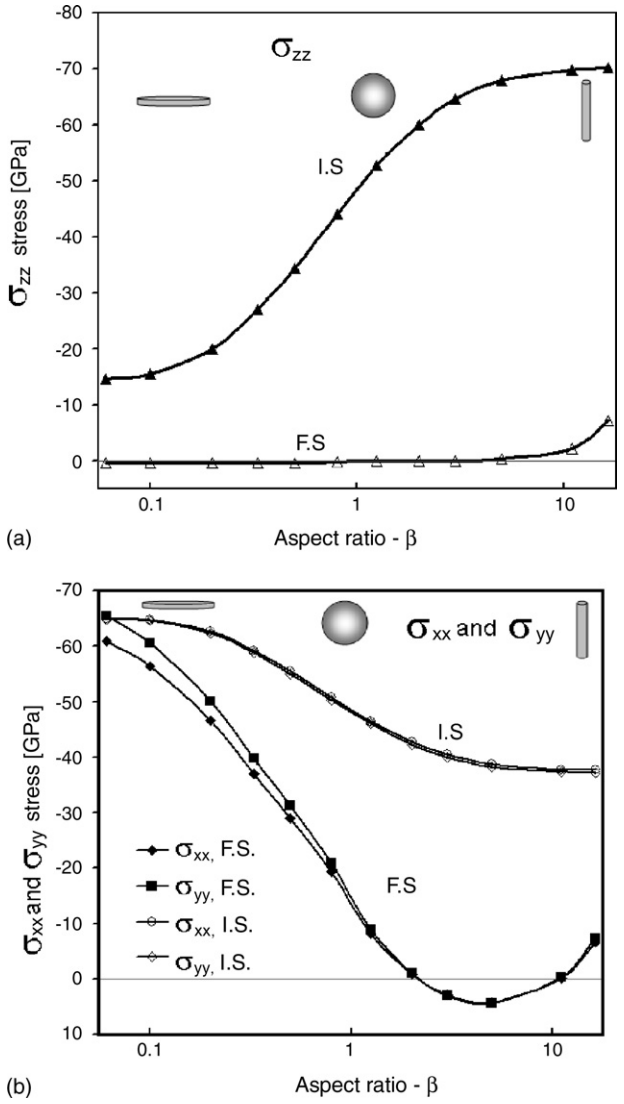

Fig. 2. The stresses at the center of elipsoidal hydrides in a homogenous matrix M_1 at the free surface (FS) calculated by the FEM and in an infinite space (IS) calculated by the semi-analytic Fourier method, as functions of the aspect ratio of the elipsoid. (a) σ_{zz} stress. (b) σ_{xx} and σ_{yy} stresses for unit transformation strain. From symmetry the difference between σ_{xx} and σ_{yy} should vanish. Both stresses are shown as an estimate of the computational error.

in an infinite matrix (Fig. 5a). Along the normalized z-axis of hydrides with smaller aspect ratio σ_{zz} rises more moderately. In particular, the maximum σ_{zz} in a half-spherical hydride is considerably lower near a free surface, relative to its value in an infinite matrix.

Figs. 5b–d illustrate the lateral stress component σ_{xx} along the direction x for the three shapes of hydrides in a half-infinite space. The plate-shaped hydride is exposed to the free surface at its broad face, but its opposite face is still coherently bounded to the underlying matrix (Fig. 4b). To avoid long-range strains in the matrix, the thin plate is rigidly constrained in the lateral directions like the plate in an infinite matrix. Fig. 5b shows that the affect of the free surface on the lateral stress in a plate-shaped hydride is small. Fig. 5b shows also the stresses in plate-shaped precipitates with different stiffnesses. The strain in the plane of the plate remains approximately $(-\varepsilon^0)$ in all the cases, thus, the σ_{xx} stress is directly proportional to the elastic constants of the precipitate. A spherical hydride is a rigid shape. The proximity to the surface allows it to release much of its internal stresses (Fig. 4c). Fig. 5c compares the lateral stresses in a spherical hydride embedded in an infinite matrix to the half-spherical hydride near a free surface. Despite the small magnitude of the stress at the center of the hydride, σ_{xx} rises near the hydride–matrix interface. The relaxation of the hydride against its periphery compresses the surrounding matrix and creates large compressive stresses in the matrix. The σ_{xx} in the hydride rises near the hydride–matrix interface due to the continuity of the radial stress required by the boundary conditions. As in the case of a plate-shaped hydride, the stresses decrease with decreasing elastic stiffness of the hydrides. The needle-shaped precipitate benefits a little from the proximity of the free surface

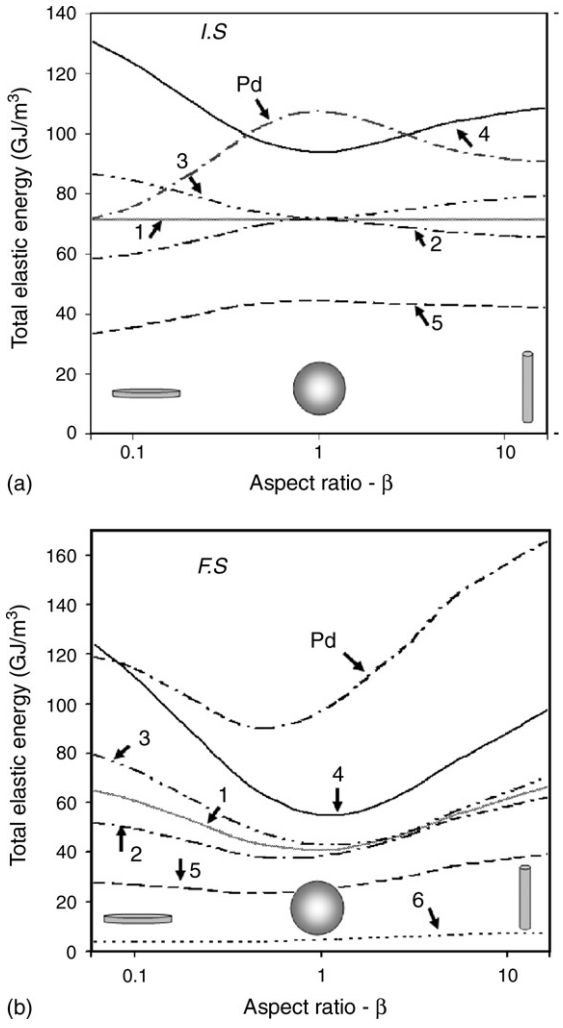

Fig. 3. Summary of the calculations of the total elastic energy (in an elipsoidal hydride and the matrix) of several systems as function of the aspect ratio of the hydride and the type of material. The energy is normalized by the volume of the hydride and the square of the transformation strain $(\varepsilon^0)^2$. (a) Infinite system (IS), (b) near a free surface (FS). Homogenuous systems curves are: (1) M_1 ($A=1$), (2) M_2 ($A=2$), (3) M_3 ($A=0.5$) and Pd ($A=2.84$). Hetrogenuous systems with a common matrix made of material M_1 and different precipitates are: (4) $C_{pre}=2C_{mat}$, (5) $C_{pre}=0.4C_{mat}$, (6) $C_{pre}=0.05C_{mat}$.

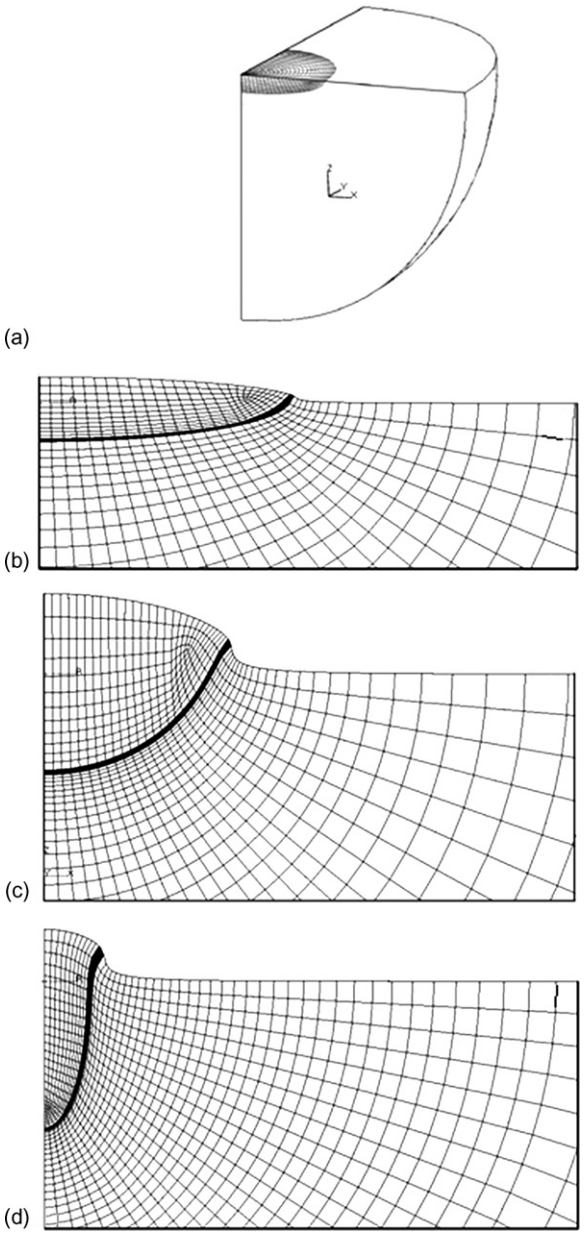

Fig. 4. The FEM model for the calculation of the energy of hydride precipitated near a free surface is a sector of the real system (a). The deformation is visualized by the displacement of the grid in the x–z plane. The initial grid is not cubic and uniform as the grid used to draw Fig. 1. The elements are refined along the matrix–hydride interface that is emphasized by a heavy line in (b–d). (b) A disk-shaped ($\beta \cong c/a \cong 5$), (c) nearly a sphere ($\beta \cong 0.8$) and (d) a needle-shaped hydride ($\beta \cong 0.2$). The transformation strains are exaggerated in purpose to illustrate the different kinematics.

since only its narrow section is exposed to the surface (Fig. 4d). The σ_{xx} in needle-shaped hydrides exhibit behavior similar to the other shapes near the free surface (Fig. 5d). However, an interesting anomalous dependence on the elastic constants is exhibited by the relatively hard hydride: σ_{xx} decreases in absolute value more than that of the softer hydride. This may be explained as a result of the lower compressibility of the hard hydride. A hard needle-shaped hydride is spooled-out of the matrix as indicated by Fig. 4d, allowing a larger relaxation of the lateral compressive stresses on the free surface.

3.2.2. Elastic energy in a homogenous system

When a half of the matrix is removed to create a half-space, much energy is released by relaxation at the free surface. The proximity of a free surface allows the largest relaxation in the case of a half-spherical hydride since as shown in Fig. 1c for infinite material and in Fig. 4c for a half-space, a spherical precipitate transfers most of its elastic energy to the surroundings.

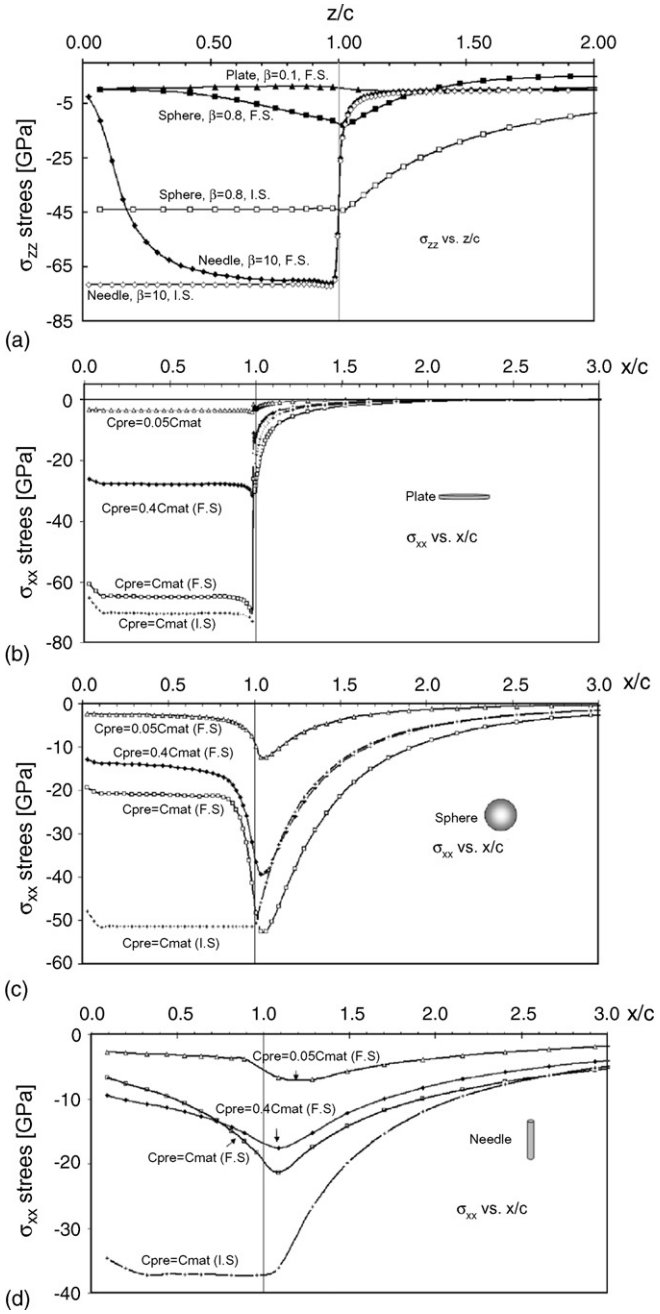

Fig. 5. Stress distribution as a function of the hydride shape, elastic heterogeneity and proximity of a free surface. (a) Profiles of the stress σ_{zz} along the z-axis of symmetry of a plate, sphere and a needle-shaped hydrides, normal to the free surface (FS) and in an infinite space (IS). (b–d) Profiles of the stress σ_{xx} along the x-axis parallel to the free surface. The plots compare the stresses in an infinite space (IS) to those associated with a free surface (FS) for several stiffness ratios: (b) plate-shaped hydride, (c) hemisperical hydride and (d) needle-shaped hydride. All the matrices in this figure are M_1. All stresses are reported per unit transformation strain.

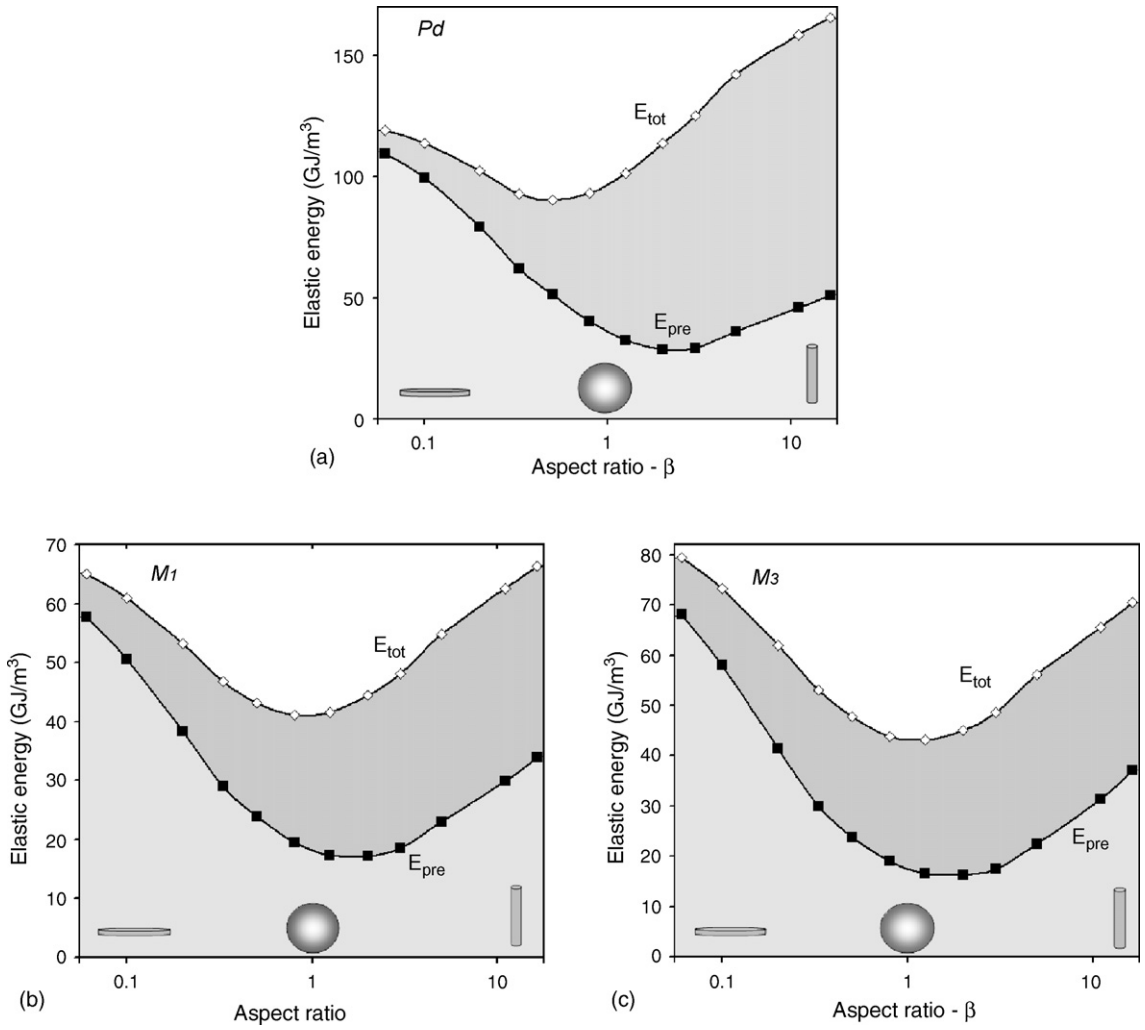

Fig. 6. The elastic energy as a function of the shape of the elipsoidal hydride at the free surface for different degrees of *anisotropy*. The energy is normalized by the volume of the hydride and the square of the transformation strain $(\varepsilon^0)^2$. Elastic homogeneity is assumed. The elastic anisotropy is $A = 2.84$ (Pd) (a), $A = 1$ (M_1) (b) and $A = 0.5$ (M_3) (c). The top line in each figure is the total elastic energy in the system (hydride and the matrix—E_{tot}). The lower lines represent the energies residing in the hydride (shaded by light gray—E_{pre}). The difference between the lines (shaded by gray) is the energy in the metal matrix.

The needle and the plate do not benefit much from the proximity of the free surface due to the *kinematic* constraints imposed on each of them along their wide dimensions. Results of energy calculations are presented in Figs. 3b and 6b as the total elastic energy associated with a unit volume of hydride per unit transformation strain. The results show a considerable reduction of the total energy in the case of spherical hydrides and a small decrease of the total energy in the cases of needle and plate hydrides, when compared with the situation of an infinite matrix. Accordingly, the preferred shape of a coherent hydride close to the free surface in an elastically homogenous system is a half sphere. Moller et al. [36] also found that a half-spherical precipitate near a free surface is associated with minimum elastic energy.

3.2.3. Homogeneous, anisotropic material

We consider a material having cubic symmetry with parallel crystallographic and specimen axes, namely the crystallographic axis [0 0 1] being parallel to the normal to the free surface, z and parallel crystallographic axes of the matrix and hydride. When $A = 2C_{44}/(C_{11}-C_{12}) > 1$, the material is soft along the ⟨1 0 0⟩ axes (C_{11} is minimal) and it is hardest along the ⟨1 1 1⟩ axes (C_{11} is maximal). Along the ⟨1 1 0⟩ axes C_{11} obtains an intermediate value. Thus the (0 0 1) planes are the softest planes in the crystal. A half-spherical hydride contains all the crystallographic axes uniformly. As the hydride becomes oblate the elastic strains in its broad face increase. This is a kinematic effect that is not sensitive to the magnitude of the elastic constants. When the broad face is a (1 0 0) plane that contains the softest crystallographic axes, the strains imposed in the plane cause small stresses and therefore the elastic energy decreases. Thus the minimum of the total energy moves slightly toward the aspect ratio of 0.8 for $A = 2$ and 2.84 (Figs. 3b and 6a). This reflects the compromise between the kinematic advantage of the sphere and the advantage of the soft (1 0 0) plane due to the elastic anisotropy.

Consider now a material with $A < 1$ and the broad face of a plate-shaped precipitate that is parallel to the (0 0 1) plane. This plane contains two ⟨1 0 0⟩ directions that are now the hardest directions, giving rise to an increase of the energy of a plate-shaped precipitate. Therefore, the energy of the spherical hydride creates deeper minimum (Figs. 3b and 6c).

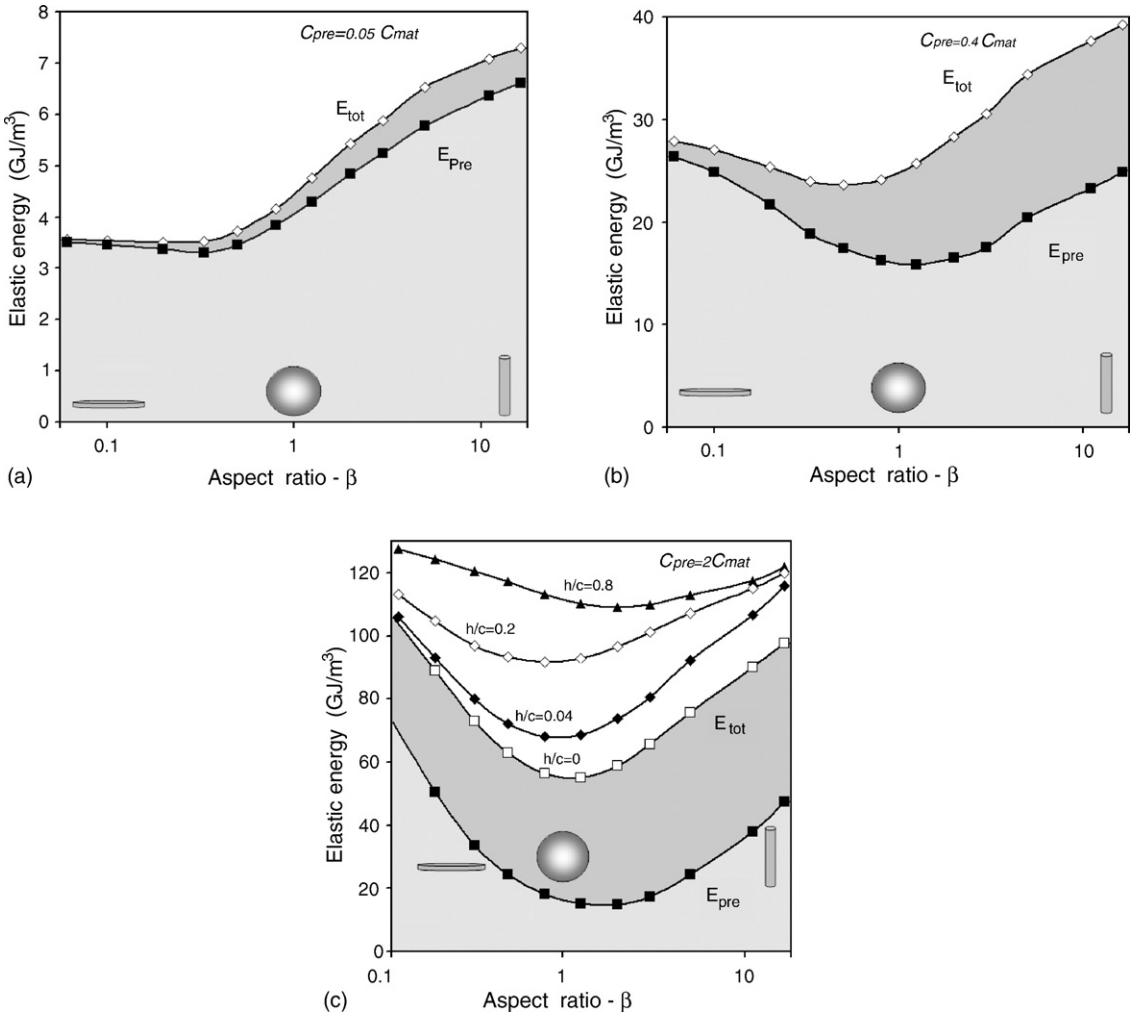

Fig. 7. The elastic energy as a function of the aspect ratio of a precipitate at the free surface in *hetrogenous* systems. Normalized by the volume of the hydride and the squar of the transformation strain $(\varepsilon^0)^2$. Elastic isotropy is assumed. The matrix is M_1. The line and shading conventions are as in Fig. 6. (a) The stiffness of the hydride is 5% that of the matrix. (b) The stiffness of the hydride is 40% that of the matrix. (c) The stiffness of the hydride is twice that of the matrix. Superimposed on part (c) are three curves describing the total elastic energy of metal–hydride systems covered with an *oxide layer*. The oxide is MO (in Table 1). The ratio of oxide thickness h to the c-axis of the hydride is kept constant along each of the curves. This implies a constant ratio between the volume of the oxide covering the hydrides and the volume of the hydride.

3.2.4. Heterogeneous system

Real systems are elastically heterogeneous, namely, the elastic constants of the matrix and the hydride are different. This can alter the preferred morphologies. Only limited data exists regarding the elastic constants of hydrides. Among then the elastic constants of $PdH_{0.66}$ were exactly measured, and found to be smaller by a factor of 0.9 than those of Pd [32]. Regarding other hydrides, e.g., $LaAl_xNi_{5-x}$, the ratio of Debye temperatures of the intermetallic compound and its hydride was used to estimate the ratio of elastic constants [37]. It was estimated that hydrides are softer than the respective metals by a factor of 0.4–0.7. Recently, the bulk modulus of GdH_2 was measured and found to be larger than that of the metal by a factor of 2 [33]. Therefore, we study two cases: one of a soft hydride relative to the matrix and a second with a hydride that is hard relative to the matrix, with all elastic constants of the hydride being multiples of the respective constants of the matrix by the same factor.

A soft hydride contains less elastic energy than a hard one with similar misfit strain, according to Eq. (3). Therefore, the total unrelaxed energy of a system that contains a soft hydride is small relative to a homogenous system, as can be seen for all shapes in Figs. 6b and 7. Among the precipitate shapes, those that impose large strains in the hard matrix, give rise to large energy in the matrix, and therefore large energy of the whole system. This is the case for the spherical and the needle-shaped hydrides. Therefore, the shape associated with minimum elastic energy shifts slightly from the shape of a sphere toward the shape of a plate. It is interesting to determine at which degree of elastic heterogeneity the minimum energy will shift from the spherical shape to a plate-shape. This will reflect the compromise between two mechanisms of saving energy: the one is due to relaxation at the free surface and the other due to softening of the hydride. Fig. 7a and b show that for $C_{ij}^{\text{pre}} = 0.4C_{ij}^{\text{mat}}$, the elastic energy associated with the plate-shape is significantly reduced but only below $C_{ij}^{\text{pre}} = 0.05C_{ij}^{\text{mat}}$ the plate-shape becomes the

shape associated with minimum energy. This 20-fold reduction of the elastic constants is indeed unrealistic, therefore equiaxed hydrides are expected to be observed experimentally.

When the hydride is hard (Fig. 7c), the total energy increases relative to a homogenous system. The minimum of the total energy remains with the spherical hydride, only the fraction of the energy in the hydride decreases since it is less constrained. It is interesting to note that also the needle-shaped hydride contains a reduced portion of the energy relative to the matrix. This is attributed to the matrix being strained in all the radial directions in the x–y plane.

3.2.5. Oxidized surface, homogenous system

The surfaces of real materials are often oxidized. Addition of a stiff oxide layer on the free surface retards the strain relaxation of the hydride and gives rise to an increase of the total elastic energy of the system. The increase of energy grows with increasing the thickness of the oxide layer. It is most significant when the hydride is spherical, which is easily explained in the framework developed above. This reaction moderates the dependence of the energy on the hydride shape (Fig. 7c). Hence, the preference of a spherical shape is less pronounced for the hydrides that are smaller relative to the oxide thickness. However, as the hydride grows, for a given oxide thickness, the contribution of the oxide to the total energy is diminishing and again the spherical shape is preferred.

3.2.6. Hyperelastic material behavior

The total strain energy in isotropic and homogenous hydride–matrix is calculated in neohookean hyperelastic model with kinematics of large displacements and large strains. The misfit strains were taken as 6% (resembling the formation of GdH_2 [34]) and 20% (resembling the formation of UH_3 [38]). The results in Table 2 show that the effect of the large displacements on the total strain energy is small and cannot cause a change in the preferred shapes.

3.2.7. Half-space elastic–plastic matrix—unoxidized surface

Often the stress generated by the precipitate exceeds the yield stress of the matrix. Plastic deformation significantly alters the strain energy. The total strain energy defined as the sum of elastic energy and plastic work was calculated for an isotropic elastic–plastic half-space embedding an elastic hydride precipitate.

It is found that the total strain energy decreased by more than one order of magnitude relative to elastic systems, out of which the elastic energy residing in the precipitate decreased by more than two orders of magnitude. The *decrease* in the strain energy is less for the case of plate-shaped precipitates and is particularly large for the case of the spherical precipitate; hence, the minimum in the energy associated with a spherical shaped particle is now very profound (Fig. 8). It is also shown in Fig. 8 that the strain energy is determined by the plastic work on the matrix while the remaining elastic energy in the precipitate is negligible.

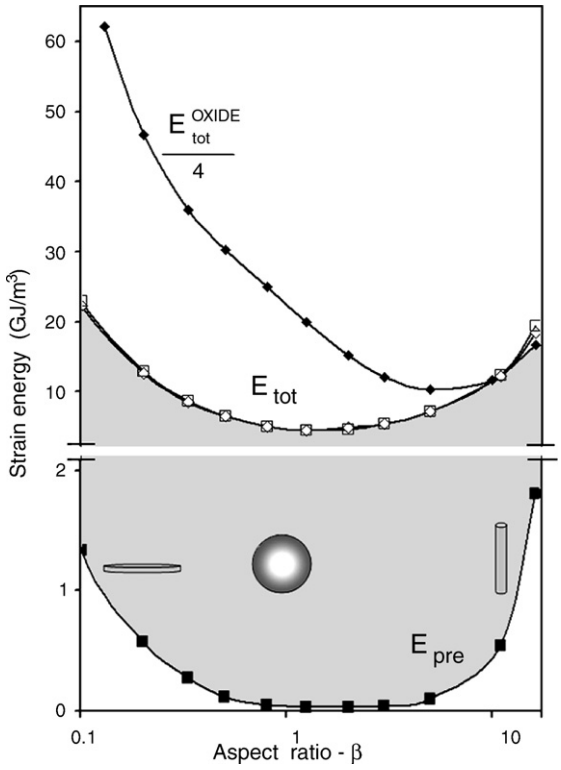

Fig. 8. The strain energy (elastic energy + plastic work) as function of the aspect ratio of elipsoidal hydrides of Gd at the free surface. Elastic isotropy is assumed. The middle lines E_{tot} (overlapping) are the total strain energy in two systems: (□) elastically homogenous system and (◊) a heterogeneous system where the stiffness of the hydride is twice that of the matrix. The lower line represents the energies residing in the hydrides (E_{pre}). The difference between the lines is the work done on the metal matrices. The top line is the total elastic strain energy in the elastic–plastic metal, elastic hydride and in the elastic oxide layer. The ratio of oxide thickness h to the c-axis of the hydride is $h/c = 0.8$. Note the changes in scales.

For the plate-shaped precipitate, one can compare two possibilities as in Section 3.1: (a) the precipitate is relaxed in its broad face (Fig. 1a). (b) The hydride is constrained nearly to its original dimensions in its broad face (Fig. 1b). In the second case, most of the energy in the system will reside in the precipi-

Table 2
The total strain energy of isotropic and homogenous hydride–matrix systems for three hydride shapes, calculated by non-linear and linear models for two misfit values

Hydride shape	Linear misfit—6%			Linear misfit—20%		
	Linear MJ/m^3	Non-linear MJ/m^3	Difference (%)	Linear MJ/m^3	Non-linear MJ/m^3	Difference (%)
Plate ($\beta = 0.06$)	236	238	0.8	8670	8940	3.1
Sphere ($\beta = 0.8$)	151	146	−3.3	5640	5110	−9.4
Needle ($\beta = 16.3$)	243	240	−1.2	8910	8570	−3.8

tate as was preferred in the elastic matrix. In the first possibility, long-range strains will be set up in the matrix. Now, since the matrix is plastic, the strain caused in it will set up relatively small stresses and therefore be associated with relatively small work. Indeed Fig. 8 shows that the strain energy in the plate-shaped precipitate is very low and the work performed on the matrix is much higher, opposite to the distribution of energy in the elastic systems.

A spherical precipitate is a compact shape that transfers much energy to the surrounding matrix in the elastic systems. An elastic precipitate in a plastic matrix is relaxed to a larger extend. Yet the plastic work done on the matrix by the spherical hydride is very small compared with a plate-shaped precipitate. This is simply due to the plate being much wider than the sphere, giving rise to much longer range coherency strains in the matrix (Fig. 1a). Thus, the spherical shape is again the preferred shape.

3.2.8. Half-space elastic–plastic matrix—oxidized surface

An elastic oxide layer adhering to a half-space with elastic–plastic matrix and elastic hydride precipitate, hinders the strain relaxation of the precipitate and thus gives rise to an increase of the strain energy in all the calculated cases (Fig. 8). The smallest effect was seen on the needle-shaped precipitate, covered by the oxide layer only at its top narrow section. Therefore, the energy becomes minimal for precipitates tending to adopt a needle-shape, perpendicular to the free surface. Increase of the strain energy as a result of the existence of an oxide layer is noticeable in particular for the plate-shaped hydride, because the oxide restricts the strain relaxation in the direction perpendicular to the plate. Stress concentration in the oxide layer that is noticeable in the edges of the hydrides is likely to cause cracks in the oxide (Fig. 5c). This phenomenon may be important during the growth of hydrides [3–6] and it deserves further study.

4. Conclusions

4.1. Linear elastic regime

The shapes of precipitates at a free surface that are associated with minimum elastic energy were determined at various situations. They were interpreted from consideration of the kinematics of the deformation and the resulting distribution of energy between the hydride and the matrix.

(a) The elastic energy of *half-spherical* hydrides at the free surface is minimal practically in all the systems considered. Exceptions from this rule are hydrides that are significantly soft relative to the matrix at the plane parallel to the free surface, where plate-shaped precipitates are preferred. Since the discussed energies are normalized by the volumes of the precipitate, the shapes associated with the minima of the elastic energy will not change during the growth of the precipitate.
(b) Existence of an oxide layer over the free surface causes an increase of the total energy of the system, with the spherical shape inducing the most significant increase in energy. Hence, when the hydride size is small relative to the oxide thickness, the elastic energy is almost indifferent to the shape of the hydride. However as the hydride grows the contribution of the oxide to the total energy is diminished and the preference of the spherical shape becomes significant.

4.2. Non-linear elastic regime

Taking into account the large displacements associated with the formation of hydrides it is found that their effect on the total strain energy is minor and the same preferred shapes obtained for the linear regime are expected.

4.3. Plastic regime

(a) Plastic yielding of the half-space while the hydride remains elastic, gives rise to a significant decrease of the total strain energy. This decrease in the strain energy is the largest for a spherical precipitate.
(b) Existence of an oxide layer over the free surface causes the preferred shape to change form a sphere to a needle perpendicular to the free surface.

Acknowledgment

The authors acknowledge support by the Germany–Israel Foundation for scientific research.

References

[1] K. Tanaka, S. Okazaki, T. Ichitsubo, T. Yamamoto, H. Inui, M. Yamaguchi, M. Koiwa, Intermetallics 8 (2000) 613–618.
[2] G.H. Kim, C.H. Chun, S.G. Lee, Acta Metall. Mater. 42 (1994) 3157–3161.
[3] J. Bloch, F. Simca, M. Krupp, A. Stern, D. Shmariahu, Z. Hadari, M.H. Mintz, J. Less-Common Met. 103 (1984) 163–171.
[4] R. Arkush, A. Venkert, M. Aizenshtein, S. Zalkind, D. Moreno, M. Brill, M.H. Mintz, N. Shamir, J Alloys Compd. 244 (1996) 197–205.
[5] M. Brill, J. Bloch, D. Shmariahu, M.H. Mintz, J. Alloys Compd. 231 (1995) 368–375.
[6] Y. Ben-Eliyahu, M. Brill, M.H. Mintz, J. Chem. Phys. 111 (1999) 6053–6060.
[7] A.G. Khachaturyan, Theory of Phase Transformations in Solids, Wiely, New York, 1983 (chapters 7 and 8).
[8] Z. Nishiyama, Martensitic Transformation, Academic Press, New York, 1973 (chapters 1 and 2).
[9] J.S. Lee, in: Y. Masumoto, T. Takagahara (Eds.), Semiconductor Quantum Dots, Physics, Spectroscopy and Applications, Springer, Stuttgart, 2002 (chapter 1).
[10] F.R.N. Nabarro, Proc. R. Soc. Lond. A 175 (1940) 519–538.
[11] R. Shneck, S.I. Rokhlin, M.P. Dariel, J. Non-Cryst. Solids 87 (1986) 263–280.
[12] J.D. Eshelby, in: N.I. Sneddon, R. Hill (Eds.), Progress in Solid Mechanics, vol. 2, Amsterdam, North Holland, 1961, p. 89.
[13] R.J. Asaro, D.M. Barnett, J. Mech. Phys. Solids 23 (1975) 77–83.
[14] T. Mura, Micromechanics of Defects in Solids, Martinus Nijhoff Publishers, Kluwer academic pub, Dordrecht, 1993 (chapters 1–3).
[15] R.D. Mindlin, D.H. Cheng, J. Appl. Phys. 21 (1950) 926–933.
[16] J.H. Davies, J. Appl. Mech. 70 (2003) 655–660.
[17] L.Z. Wu, Y.S. Du, J. Appl. Mech. 63 (1996) 925–932.
[18] R. Shneck, A. Brokman, M.P. Dariel, Modell. Simul. Mater. Sci. Eng. 3 (1995) 235–251.
[19] K. Seo, T. Mura, Trans. ASME: J. Appl. Mech. 46 (1979) 568–572.
[20] Y.P. Chiu, Trans. ASME: J. Appl. Mech. 45 (1978) 302–306.
[21] F. Glas, Philos. Magn. A82 (2002) 2591–2608.
[22] H.Y. Yu, S.C. Sanday, J. Appl. Mech. 57 (1990) 74–77.
[23] E. Pan, B. Yang, J. Appl. Phys. 90 (2001) 6190–6196.
[24] F. Laszlo, J. Iron Steel Inst. 164 (1950) 5–25.

[25] J.K. Lee, D.M. Barnett, H.I. Aaronson, Metal. Trans. 8A (1977) 963–970.
[26] R. Schneck, S.I. Rokhlin, M.P. Dariel, Metal. Trans. 16A (1985) 197–202.
[27] I.S. Suh, J.K. Park, Scripta Metal. 33 (2) (1995) 205–211.
[28] (a) A.L. Roitburd, Sov. Phys. Solid State 28 (1986) 1716–1718;
(b) A.L. Roitburd, Solid State 24 (1984) 1224–1233.
[29] U. Dahmen, K.H. Westmacott, Script. Metal. 34 (1986) 475–482.
[30] R. Nunes, et al., ASM Handbook, Properties and Selection: Nonferrous Alloys and Special-Purpose Materials, ASM International, vol. 2, 1991, p. 1181.
[31] D. Balestrieri, Y. Philipponneau, G.M. Decroix, Y. Jorand, G. Fantozzi, J. Eur. Ceram. Soc. 18 (1998) 1073–1077.
[32] D.K. Hsu, R.G. Leisure, Phys. Rev. B 20 (4) (1979) 1339–1344.
[33] I. Halevy, private communication, 2003.
[34] M. Brill, I. Halevy, G. Kimmel, M.H. Mintz, J. Bloch, J Alloys Compd. 330–332 (2002) 93–98.
[35] M.A. Crisfield, Non Linear Finite Element Analysis of Solids and Structure, J. Wiely, NY, 2000.
[36] J. Moller, J.W.P. Schmelzer, I. Gutzow, Nucleation Theory and Applications, Joint Institute for Nuclear Research, Dubna, 1999, pp. 464–491.
[37] M. Bereznitsky, A. Ode, J.E. Hightower, O. Yeheskel, I. Jacob, R.G. Leisure, J. Appl. Phys. 91 (8) (2002) 5010–5015.
[38] R.E. Rundle, J. Am. Chem. Soc. 69 (1947) 1719–1723.